

A quantitative analysis of Gravitational Wave spectrum sourced from First-Order Chiral Phase Transition of QCD

Hui-wen Zheng,^{1,*} Fei Gao,^{2,†} Ligong Bian,^{3,4,‡} Si-xue Qin,^{3,§} and Yu-xin Liu^{1,4,5,¶}

¹*Department of Physics and State Key Laboratory of Nuclear Physics and Technology, Peking University, Beijing 100871, China.*

²*School of Physics, Beijing Institute of Technology, 100081 Beijing, China*

³*Department of Physics and Chongqing Key Laboratory for Strongly Coupled Physics, Chongqing University, Chongqing 401331, China.*

⁴*Center for High Energy Physics, Peking University, Beijing 100871, China.*

⁵*Collaborative Innovation Center of Quantum Matter, Beijing 100871, China.*

(Dated: July 8, 2024)

We investigate the cosmological first-order chiral phase transition of QCD, and for the first time calculate its parameters which can fully determine the gravitational wave spectrum. With the state-of-the-art calculation from the functional QCD method, we found that the large chemical potential of QCD phase transition results in very weak and fast first-order phase transitions at the temperature lower than $\mathcal{O}(10^2)$ MeV. These results further suggest that the GW signals of NANOGrav are very unlikely sourced from the chiral phase transition of QCD.

Keywords: gravitational waves, cosmic QCD transition, lepton asymmetry, functional QCD

Introduction. The space-based interferometers, such as μ Ares [1], Taiji [2, 3], Tianqin [4, 5], the Laser Interferometer Space Antenna (LISA) [6, 7], the Big Bang Observer (BBO) [8–10] and the Deci-Hertz Interferometer Gravitational Wave Observatory (DECIGO) [11–14], offer a frequency window from 10^{-7} Hz to 10 Hz for detecting the stochastic gravitational waves background (SGWB). Moreover, the evidences of the SGWB at nanohz are detected by the pulsar timing arrays (PTA) collaborations, including the North American Nanohertz Observatory for Gravitational Waves (NANOGrav) [15, 16], the European Pulsar Timing Array (EPTA) [17, 18], the Parkes Pulsar Timing Array (PPTA) [19, 20], the International Pulsar Timing Array (IPTA) [21], and the Chinese Pulsar Timing Array (CPTA) [22]. The generation mechanism of SGWB is a highly debated topic with enormous models being applied to explain the measurements which include supermassive black hole binaries (SMBHBs) [15, 23–26], curvature perturbations [27, 28], and new-physics models including first-order phase transition (FOPT) [29–50], cosmic strings [51–58], and domain walls [59–69], etc. Amongst the studies, it has been estimated that the SGWB can be induced by a strong FOPT at about $T_* \sim 1 - 10$ MeV [70–72], which makes the cosmic QCD phase transition (PT) a competitive candidate. Moreover, the recent studies suggest that the large lepton asymmetries can induce the QCD FOPT in early Universe, and by themselves give the observed value of baryon asymmetry via the so called “sphaleron freeze-in” mechanism [73, 74]. Thus, a strong QCD phase transition may be a simple solution for multiple problems in cosmology.

The nonperturbative nature of QCD makes it difficult to study its PT dynamics, especially, the quantitative information of thermodynamics quantities and the ef-

fective potential of QCD are still not very clear. Very recently, the quantitative truncation scheme together with the computation of thermodynamics quantities are reached [75], and a novel method to determine the effective potential was proposed in Ref. [76]. These progresses make the quantitative analysis of the QCD PT viable through the functional QCD approaches, specifically, the Dyson-Schwinger equation (DSE) [75–83]. For the first time, we show that one can quantitatively determine the strength, the duration, and the percolation temperature T_* of the QCD PT. We then compute the gravitational waves (GWs) spectrum from QCD PT and found that the signal from QCD PT is not possible to match with the NANOGrav measurements, and moreover, the PT is also too weak to produce detectable GW signals for the current and the being constructed GW detectors in the frequency range from nanohertz to hertz.

Cosmic trajectories crossing the QCD PT. In the QCD epoch, the baryon number Y_B , the individual lepton flavour number Y_{L_f} , and the electric charge Q asymmetry can be considered as the conserved quantities during the QCD PT [84]. Thus, without any further assumptions, one can consider the conservation equations:

$$Y_{L_f} = \frac{n_f + n_{\nu_f}}{s}, \quad (1a)$$

$$Y_B = \sum_i \frac{B_i n_i}{s}, \quad (1b)$$

$$Q = \sum_i \frac{Q_i n_i}{s}, \quad (1c)$$

with s the total entropy density of the Universe, n_i the net number density (i.e., the particle minus the anti-particle number density of the species i), $f = (e, \mu, \tau)$,

$i = (e, \mu, \tau, u, d, s, c)$, B_i the baryon number of species i , Q_i the electric charge of species i , $Y_B = 8.7 \times 10^{-11}$ the observed baryon asymmetry [85], $Q = 0$ the charge neutrality for universe. Y_{L_f} is less constrained, allowing for a larger lepton asymmetry, provided it satisfies the big bang nucleosynthesis (BBN) and the cosmic microwave background (CMB) constraint $|Y_{L_e} + Y_{L_\mu} + Y_{L_\tau}| < 1.2 \times 10^{-2}$ [86–91]. Under this constraint, the individual Y_{L_f} will decrease once the neutrino oscillations start at $T_* \sim 10$ MeV [92–94]. Therefore, the large lepton asymmetries exist only for $T_* > 10$ MeV. For $T_* < 10$ MeV, the diminished Y_{L_f} will lower the lepton and the quark chemical potentials to satisfy the BBN constraint.

Under the conditions of the kinetic and the chemical equilibrium [84], the net leptons and the photons number densities are expressed by Fermi-Dirac distributions and Bose-Einstein distributions, respectively. In the QCD sector, the nonperturbative property prevents the QCD matter from being simply represented by Fermi-Dirac and Bose-Einstein distributions. Therefore, we apply the DSE to accomplish the complete calculations of the QCD phase diagram, the thermodynamic quantities and especially here the effective potential, which is for the first time obtained and applied to compute the gravitational wave signals. Firstly, in the current scheme one obtains the critical end point (CEP) at $(T^E, \mu_q^E) = (101.3, 186.0)$ MeV [76]. Moreover, with the effective potential obtained from the homotopy method, it is able to determine the first-order phase transition (FOPT) line, on which the chiral symmetric (Wigner) phase and the chiral symmetry breaking (Nambu+) phase degenerate.

The scenario ($Y_{L_e} = 0, Y_{L_\mu} = -Y_{L_\tau}$) is the main focus of this work, which satisfies the BBN constraints and can induce the FOPT of QCD [73, 95]. In this scenario, Fig. 1 illustrates the dependence of cosmic trajectory on Y_{L_μ} , where $Y_{L_\mu} = -0.22$ represents the critical value to trigger the FOPT, which is consistent with the previous study [74]. As Y_{L_μ} decreases gradually from -0.14 to -0.22 , the cosmic trajectory quickly approaches to CEP, which is caused by the strengthening of PT as approaching CEP. When $Y_{L_\mu} < -0.22$, the cosmic trajectory steps into the FOPT region.

When the cosmic trajectory crosses the QCD FOPT, there can be GW emission during the bubble nucleation. This is a non-equilibrium process which includes the false-vacuum-dominated stage and the supercooling stage, represented by the solid line and the dashed line respectively in Fig. 1. Before the nucleation, the dynamics can be studied with the QCD effective potential at hand, which will be explained in detail in the next section. After the nucleation, when the part of the Universe is converted to the true vacuum, the entropy of the system is not conserved anymore due to the non-equilibrium effect. The upper bound of the cosmic trajectory, i.e., the gray dot-dashed line below, is determined under the condition that s/n_q is conserved after the PT as depicted

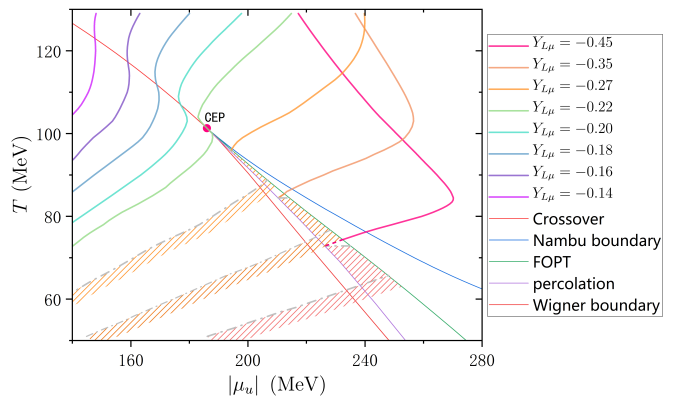


FIG. 1. Cosmic trajectories in the scenario $Y_{L_e} = 0$ and $Y_{L_\mu} = -Y_{L_\tau}$ in QCD phase diagram. The cosmic trajectories intersect the FOPT line at (T_c, μ_c) and the percolation line at (T_*, μ_*) . Solid line: the specific cosmic trajectory; dashed line: the supercooling stage for a cosmic trajectory before the percolation and after the FOPT; gray dot-dashed line: the upper bound for the possible cosmic trajectory; shadow region: an area through which a cosmic trajectory may pass.

in Fig. 1. However, the complete determination requires to further consider the dynamics of the FOPT which is under progress. A detailed illustration of the evolution of the cosmic trajectory is presented in the supplemental material.

PT parameters. With the mechanism of the QCD FOPT, one can expect the generation of the GWs. We consider the sound-waves-only analysis (PT-SOUND) for the GW because our subsequent calculation shows that the bubble walls cannot runaway. The PT-SOUND GW spectrum is written as [70, 96–102]:

$$\Omega_s(f) = \mathcal{D} \tilde{\Omega}_s \Upsilon(\tau_{sw}) \left(\frac{\kappa_s \alpha_*}{1 + \alpha_*} \right)^2 (H_* R_*) \mathcal{S}(f/f_s), \quad (2)$$

with α_* the PT strength, $\beta/H_* = (8\pi)^{1/3} v_w / (H_* R_*)$ being the inverse PT duration [98] and v_w the bubble wall velocity. Both of the PT parameters requires the knowledge of the QCD effective potential, which we obtain for the first time by applying the homotopy method to the QCD theory [76]. Besides, the GWs are always generated along the percolation line, which corresponds to the percolation temperature T_* , i.e., the temperature when $\sim 34\%$ of the volume of the universe is converted into the true vacuum determined with the effective potential. These information allows us to obtain the GW spectrum.

The QCD effective potential comes from a generalized Legendre transformation to the Cornwall, Jackiw and Tomboulis (CJT) connected generating functional [76]. This transformation converts the variable of the CJT effective potential, i.e., the quark propagator, to the self-energy, which is the key point to keep the effective potential to be bounded from below [103]. The new effective

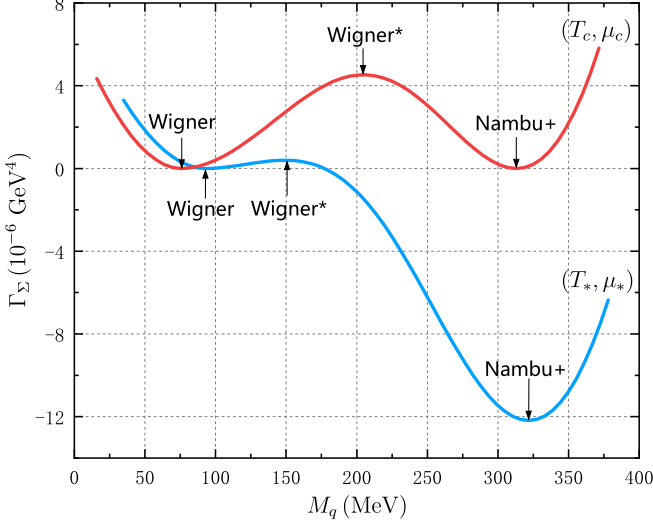


FIG. 2. The $N_f = 2$ effective potential evolving from (T_c, μ_c) to (T_*, μ_*) on the $Y_{L\mu} = -0.45$ cosmological trajectory. The dynamic quark mass M_q is the order parameter of the effective potential. The homotopy method is applied to obtain the effective potential from the DSE beyond the bare vertex approximation [76]. Here, we have defined the effective potential to be zero at the Wigner solution.

potential is written as [76]:

$$\Gamma_\Sigma[\Sigma] = \text{TrLn}[S_0^{-1} + \Sigma]^{-1} - \text{Tr}[1] - \Gamma_2[(S+L)] + \text{Tr}[(S+L)\Sigma], \quad (3)$$

with S_0 the free quark propagator, S the dressed quark propagator, $\Sigma = \Sigma[(S+L)] \equiv \frac{\delta\Gamma_2[(S+L)]}{\delta(S+L)}$ the self-energy, L the external source, and Γ_2 the sum of all two-particle-irreducible diagrams as a functional of $S+L$.

Moreover, we apply the homotopy method, i.e., a simplified version of the functional integration, to determine the effective potential from the quantitative truncation scheme of the DSE [76]:

$$\begin{aligned} \Gamma_\Sigma[M_q] &:= \Gamma_\Sigma[\Sigma_\chi] - \Gamma_\Sigma[\Sigma_0] \\ &= \int_0^x d\xi \text{Tr} \left\{ \frac{d\Sigma_\xi}{d\xi} \left[-(S_0^{-1} + \Sigma_\xi)^{-1} + S_\xi \right] \right\}, \end{aligned} \quad (4)$$

where

$$\Sigma_\xi = \Sigma[S_\xi], \quad S_\xi = [(1-\xi)S_1^{-1} + \xi S_2^{-1}]^{-1}, \quad (5)$$

with ξ being the homotopy parameter, S_1 and S_2 being the Wigner and Nambu+ solutions respectively. Moreover, the effective potential has been converted to a function of M_q by connecting the homotopy parameter to the dynamic quark mass M_q .

We firstly illustrate the QCD effective potential Γ_Σ in Fig. 2, where the Wigner vacuum is the false vacuum, the Nambu+ is the true vacuum and the Wigner* is the

unstable vacuum indicating the occurrence of FOPT. At the PT temperature T_c , the false and the true vacuum are degenerate. Vacuum bubbles merge with each other around the percolation temperature T_* . At that time, the false vacuum has an energy larger than the true vacuum.

Using the effective potential, we calculate the decay rate of the false vacuum and find that it is dominated by the thermally-induced decay rate [104–107]:

$$\begin{aligned} \Gamma(T, \mu) &\simeq T \left(\frac{S_3}{2\pi T} \right)^{\frac{3}{2}} \exp\left(-\frac{S_3}{T}\right) \\ &\quad \times \max(T^3, \mu^3, r^{-3}, (V_{\text{eff}}'')^{3/2}, \phi^3), \end{aligned} \quad (6)$$

with

$$S_3 = 4\pi \int_0^\infty dr r^2 \left[\frac{1}{2} \left(\frac{d\phi}{dr} \right)^2 + V_{\text{eff}}(\phi) \right]. \quad (7)$$

Here, S_3 is the 3-dimensional Euclidean actions for the $O(3)$ -symmetric bounce solutions, r is the bubble radius, $\phi = M_q$ is the dynamical quark mass, $V_{\text{eff}}'' = d^2V_{\text{eff}}/d\phi^2$, and $V_{\text{eff}} = \Gamma_\Sigma$ is the effective potential calculated from the DSE with the homotopy method [76].

The percolation temperature T_* is determined by the following equation:

$$\begin{aligned} I(T, \mu) &= \frac{4\pi}{3} \int_{\rho_r}^{\rho_r^c} d\rho_r' \frac{1}{4\rho_r'^{7/4}} \frac{\Gamma(T', \mu')}{H(T', \mu')} \\ &\quad \times \left(\int_{\rho_r}^{\rho_r'} d\rho_r'' \frac{v_w}{4H(T'', \mu'') \rho_r''^{3/4}} \right)^3, \end{aligned} \quad (8)$$

with (T, μ) varying along the cosmic trajectory, H the Hubble parameter, $\rho_r = \rho_r(T, \mu)$ the energy density of the radiation, ρ_r^c the energy density when the false and the true vacuum are degenerate, and v_w the bubble wall velocity, where we assume $v_w = 1$ as NANOGrav [70]. ρ_r ignores the matter because its energy density is much smaller than that of radiation. The percolation temperature T_* can then be determined by $I(T_*, \mu_*) \simeq 0.34$ and the cosmic trajectory.

The PT strength α_* depends on the available energy released from the PT, normalized to the energy densities of the background radiation:

$$\alpha_* = \left. \frac{\Delta\theta}{\rho_r} \right|_{(T_*, \mu_*)}, \quad (9)$$

with

$$\Delta\theta = \frac{1}{4}T\Delta s + \frac{1}{4}\mu_q\Delta n_q - \Delta P, \quad (10)$$

$$\rho_r(T, \mu) = \sum_a \int \frac{d^3p}{(2\pi)^3} E_a f_{F/B}(E_a, T, \mu). \quad (11)$$

Here, $E_a = \sqrt{p^2 + m_a^2}$, θ is the trace anomaly, s is the entropy density, n_q is the quark number density, $P = -\Gamma_\Sigma$

is the pressure where Δ denotes the difference between the false and the true vacuum, and ρ_r collects electron, muon, all neutrinos, photon and u/d quarks in the false vacuum, where the temperature dependence of the lepton chemical potentials along the percolation line are shown in the Appendix. A critical value α_∞ that can determine whether the bubble walls can runaway is also considered [100, 108], which sums over all particles during the PT.

For the FOPT with finite chemical potential, the inverse PT duration β/H_* can be obtained as:

$$\beta/H_* = 4\rho_r \frac{d}{d\rho_r} \left(\frac{S_3}{T} \right) \Big|_{(T_*, \mu_*)}, \quad (12)$$

where the derivative lies along the cosmic trajectory.

Numerical results. After a complete computation for the GW spectrum, we find that neither of α_* and β/H_* over the whole QCD chiral PT can be matched with the NANOGrav measurements. This has been depicted clearly in Fig. 3 which gives the comparison between the PT parameters calculated from the QCD effective potential and the sound-wave-only analysis (PT-SOUND) by the NANOGrav collaboration. Note that we only consider the sound-wave-only case because $\alpha - \alpha_\infty < 0$ is verified here. This situation prevents the runaway of bubble wave, causing the GW to be dominated by the sound waves source [109].

In detail, for α_* , its value is at least one order of magnitude smaller compared to the NANOGrav constraints. Such a small value is mainly due to the large energy density of the background radiation. The large energy density comes from the large chemical potentials of the leptons, which is a direct result of the conservation conditions in Eq. (1). In particular, the chemical potentials of the electron and electron neutrino are roughly equivalent to that of the quark, while the chemical potentials of muon neutrinos and/or tau neutrinos are more than three times the quark chemical potential. For β/H_* , the value we obtained is three orders of magnitude larger than the one to match with the analysis from NANOGrav collaboration. This is mainly because the cosmic trajectory leans more towards the chemical potential, causing the derivative of S_3/T along the trajectory to be large. Meanwhile, in the Eq. (12), ρ_r outside of the derivative also maintains a large value due to the contribution of the non-vanishing chemical potential along the percolation line. As a result, β/H_* remains significantly large.

Based on the obtained PT parameters α_* and β/H_* , we show our result of the GWs sourced from the first-order QCD PT in Fig. 4. The quantitative computation here disapproves the QCD chiral PT as a source of the SGWB to explain the signals detected by NANOGrav.

Conclusion. In this *Letter*, we calculate the cosmic trajectories at large quark chemical potential, and for the

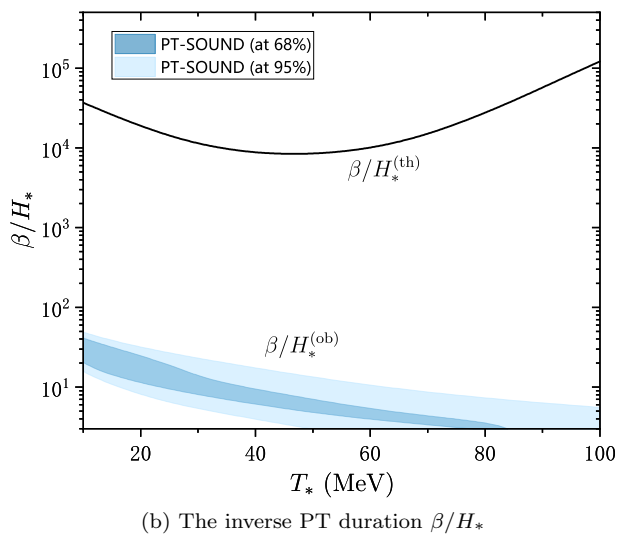
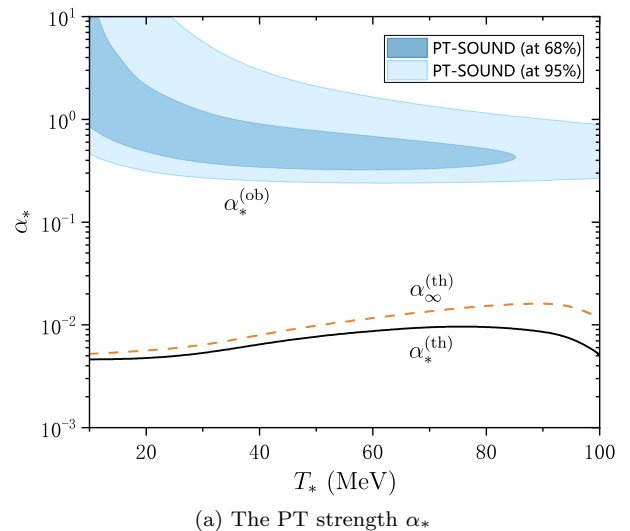


FIG. 3. The temperature dependence of the PT parameters (α_* , β/H_*) on the percolation line in the QCD phase diagram. Deep blue region: the NANOGrav constraints on the PT parameters from the PT-SOUND model (at 68% credible level); light blue region: the NANOGrav constraints on the PT parameters from the PT-SOUND model (at 95% credible level) [70].

first time quantitatively determine the PT parameters of the first-order QCD phase transitions, through their relation to the thermodynamic quantities and effective potential from the functional QCD methods.

We firstly verify that a large lepton asymmetry can induce the first-order QCD PT. We consider the scenario ($Y_{L_e} = 0, Y_{L_\mu} = -Y_{L_\tau}$), and find that the FOPT occurs when $Y_{L_\mu} < -0.22$. This conclusion is essentially from the conservation laws during the Universe evolution without further assumptions. We further compute the PT parameters via the QCD effective potential, and then determine the gravitational wave spectrum through the sound shell model.

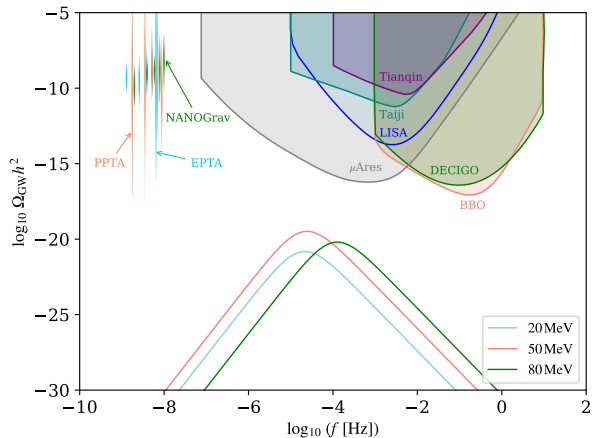


FIG. 4. The gravitational waves spectra of the first-order QCD phase transition. The violins plot the first five frequency bins of the datasets, including: EPTA [18], PPTA [20, 110, 111], and NANOGrav [16, 70, 112]. The sensitivity curves includes: μ Ares [1], Taiji [2, 3], Tianqin [4, 5], LISA [6, 7], BBO [8–10] and DECIGO [11–14].

The obtained GW spectrum makes it possible to conduct a quantitative analysis with the measurements of NANOGrav. In short, the obtained PT strength α_* is $\mathcal{O}(10^{-2})$, the inverse PT duration β/H_* is $\mathcal{O}(10^4)$. The values deviate significantly from the measurements of NANOGrav mainly due to the large energy density of the background radiation. This large energy density arises from the large chemical potentials of the leptons, which is a direct result of the conservation laws.

Finally, we illustrate the disparity between the computed GW spectra based on the PT parameters and the violin plots of the EPTA, PPTA and NANOGrav, alongside the sensitivity curves of the μ Ares, Taiji, Tianqin, LISA, BBO and DECIGO. In brief, through a quantitative determination of the QCD PT parameters, we find that a first-order chiral PT of QCD cannot produce the SGWB signal by the NANOGrav experiment. The PT is also too weak to produce detectable GW signals that can be reached by the current and the being constructed GW detectors.

Acknowledgments F.G. and H.Z. thank Isabel M. Oldengott and Yi Lu for helpful discussions. This work is supported by the National Science Foundation of China under Grants No.12175007, No.12247107 and No.12305134. L.B. is supported by the National Natural Science Foundation of China (NSFC) under Grants No. 12075041, No. 12322505, and No. 12347101. L.B. also acknowledges Chongqing Talents: Exceptional Young Talents Project No. cstc2024ycjh-bgzxm0020.

* zhenghuiwen@stu.pku.edu.cn

† fei.gao@bit.edu.cn

‡ lgbycl@cqu.edu.cn

§ sqin@cqu.edu.cn

¶ yxliu@pku.edu.cn

- [1] A. Sesana et al., *Exper. Astron.* **51**, 1333 (2021), arXiv:1908.11391 [astro-ph.IM].
- [2] W.-R. Hu and Y.-L. Wu, *Natl. Sci. Rev.* **4**, 685 (2017).
- [3] W.-H. Ruan, Z.-K. Guo, R.-G. Cai, and Y.-Z. Zhang, *Int. J. Mod. Phys. A* **35**, 2050075 (2020), arXiv:1807.09495 [gr-qc].
- [4] J. Luo et al. (TianQin), *Class. Quant. Grav.* **33**, 035010 (2016), arXiv:1512.02076 [astro-ph.IM].
- [5] K. Zhou, J. Cheng, and L. Ren, (2023), arXiv:2306.14439 [gr-qc].
- [6] P. Amaro-Seoane et al. (LISA), (2017), arXiv:1702.00786 [astro-ph.IM].
- [7] J. Baker et al., (2019), arXiv:1907.06482 [astro-ph.IM].
- [8] J. Crowder and N. J. Cornish, *Phys. Rev. D* **72**, 083005 (2005), arXiv:gr-qc/0506015.
- [9] V. Corbin and N. J. Cornish, *Class. Quant. Grav.* **23**, 2435 (2006), arXiv:gr-qc/0512039.
- [10] G. M. Harry, P. Fritschel, D. A. Shaddock, W. Folkner, and E. S. Phinney, *Class. Quant. Grav.* **23**, 4887 (2006), [Erratum: *Class. Quant. Grav.* **23**, 7361 (2006)].
- [11] N. Seto, S. Kawamura, and T. Nakamura, *Phys. Rev. Lett.* **87**, 221103 (2001), arXiv:astro-ph/0108011.
- [12] S. Kawamura et al., *Class. Quant. Grav.* **23**, S125 (2006).
- [13] K. Yagi and N. Seto, *Phys. Rev. D* **83**, 044011 (2011), [Erratum: *Phys. Rev. D* **95**, 109901 (2017)], arXiv:1101.3940 [astro-ph.CO].
- [14] S. Isoyama, H. Nakano, and T. Nakamura, *PTEP* **2018**, 073E01 (2018), arXiv:1802.06977 [gr-qc].
- [15] Z. Arzoumanian et al. (NANOGrav), *Astrophys. J. Lett.* **905**, L34 (2020), arXiv:2009.04496 [astro-ph.HE].
- [16] G. Agazie et al. (NANOGrav), *Astrophys. J. Lett.* **951**, L8 (2023), arXiv:2306.16213 [astro-ph.HE].
- [17] S. Chen et al. (EPTA), *Mon. Not. Roy. Astron. Soc.* **508**, 4970 (2021), arXiv:2110.13184 [astro-ph.HE].
- [18] J. Antoniadis et al. (EPTA, InPTA:), *Astron. Astrophys.* **678**, A50 (2023), arXiv:2306.16214 [astro-ph.HE].
- [19] B. Goncharov et al., *Astrophys. J. Lett.* **917**, L19 (2021), arXiv:2107.12112 [astro-ph.HE].
- [20] D. J. Reardon et al., *Astrophys. J. Lett.* **951**, L6 (2023), arXiv:2306.16215 [astro-ph.HE].
- [21] J. Antoniadis et al., *Mon. Not. Roy. Astron. Soc.* **510**, 4873 (2022), arXiv:2201.03980 [astro-ph.HE].
- [22] H. Xu et al., *Res. Astron. Astrophys.* **23**, 075024 (2023), arXiv:2306.16216 [astro-ph.HE].
- [23] M. Rajagopal and R. W. Romani, *Astrophys. J.* **446**, 543 (1995), arXiv:astro-ph/9412038.
- [24] E. S. Phinney, (2001), arXiv:astro-ph/0108028.
- [25] A. H. Jaffe and D. C. Backer, *Astrophys. J.* **583**, 616 (2003), arXiv:astro-ph/0210148.
- [26] J. S. B. Wyithe and A. Loeb, *Astrophys. J.* **590**, 691 (2003), arXiv:astro-ph/0211556.
- [27] K. N. Ananda, C. Clarkson, and D. Wands, *Phys. Rev. D* **75**, 123518 (2007), arXiv:gr-qc/0612013.
- [28] D. Baumann, P. J. Steinhardt, K. Takahashi, and K. Ichiki, *Phys. Rev. D* **76**, 084019 (2007), arXiv:hep-

- th/0703290.
- [29] M. Losada, *Phys. Rev. D* **56**, 2893 (1997), arXiv:hep-ph/9605266.
- [30] J. M. Cline and P.-A. Lemieux, *Phys. Rev. D* **55**, 3873 (1997), arXiv:hep-ph/9609240.
- [31] M. Laine, *Nucl. Phys. B* **481**, 43 (1996), [Erratum: *Nucl.Phys.B* 548, 637–638 (1999)], arXiv:hep-ph/9605283.
- [32] D. Bodeker, P. John, M. Laine, and M. G. Schmidt, *Nucl. Phys. B* **497**, 387 (1997), arXiv:hep-ph/9612364.
- [33] A. Neronov, A. Roper Pol, C. Caprini, and D. Semikoz, *Phys. Rev. D* **103**, 041302 (2021), arXiv:2009.14174 [astro-ph.CO].
- [34] S. L. Li, L. J. Shao, P. X. Wu, and H. Yu, *Phys. Rev. D* **104**, 043510 (2021), arXiv:2101.08012 [astro-ph.CO].
- [35] Y. Nakai, M. Suzuki, F. Takahashi, and M. Yamada, *Phys. Lett. B* **816**, 136238 (2021), arXiv:2009.09754 [astro-ph.CO].
- [36] W. Ratzinger and P. Schwaller, *SciPost Phys.* **10**, 047 (2021), arXiv:2009.11875 [astro-ph.CO].
- [37] A. Kosowsky, M. S. Turner, and R. Watkins, *Phys. Rev. Lett.* **69**, 2026 (1992).
- [38] C. Caprini, R. Durrer, and X. Siemens, *Phys. Rev. D* **82**, 063511 (2010), arXiv:1007.1218 [astro-ph.CO].
- [39] A. Addazi, Y.-F. Cai, Q. Gan, A. Marciano, and K. Zeng, *Sci. China Phys. Mech. Astron.* **64**, 290411 (2021), arXiv:2009.10327 [hep-ph].
- [40] X. Xue et al., *Phys. Rev. Lett.* **127**, 251303 (2021), arXiv:2110.03096 [astro-ph.CO].
- [41] J. Ellis, M. Lewicki, C. Lin, and V. Vaskonen, *Phys. Rev. D* **108**, 103511 (2023), arXiv:2306.17147 [astro-ph.CO].
- [42] A. Addazi, Y.-F. Cai, A. Marciano, and L. Visinelli, *Phys. Rev. D* **109**, 015028 (2024), arXiv:2306.17205 [astro-ph.CO].
- [43] T. Ghosh, A. Ghoshal, H.-K. Guo, F. Hajkarim, S. F. King, K. Sinha, X. Wang, and G. White, *JCAP* **05**, 100 (2024), arXiv:2307.02259 [astro-ph.HE].
- [44] S. Rezapour, K. Bitaghsir Fadafan, and M. Ahmadvand, *Annals Phys.* **437**, 168731 (2022), arXiv:2006.04265 [hep-th].
- [45] S. Rezapour, K. Bitaghsir Fadafan, and M. Ahmadvand, *Phys. Scripta* **97**, 035301 (2022).
- [46] M. Ahmadvand and K. Bitaghsir Fadafan, *Phys. Lett. B* **779**, 1 (2018), arXiv:1707.05068 [hep-th].
- [47] M. Ahmadvand and K. Bitaghsir Fadafan, *Phys. Lett. B* **772**, 747 (2017), arXiv:1703.02801 [hep-th].
- [48] P. Athron, A. Fowlie, C.-T. Lu, L. Morris, L. Wu, Y. Wu, and Z. Xu, *Phys. Rev. Lett.* **132**, 221001 (2024), arXiv:2306.17239 [hep-ph].
- [49] C. Han, K.-P. Xie, J. M. Yang, and M. Zhang, (2023), arXiv:2306.16966 [hep-ph].
- [50] S.-P. Li and K.-P. Xie, *Phys. Rev. D* **108**, 055018 (2023), arXiv:2307.01086 [hep-ph].
- [51] X. Siemens, V. Mandic, and J. Creighton, *Phys. Rev. Lett.* **98**, 111101 (2007), arXiv:astro-ph/0610920.
- [52] J. Ellis and M. Lewicki, *Phys. Rev. Lett.* **126**, 041304 (2021), arXiv:2009.06555 [astro-ph.CO].
- [53] S. Blasi, V. Brdar, and K. Schmitz, *Phys. Rev. Lett.* **126**, 041305 (2021), arXiv:2009.06607 [astro-ph.CO].
- [54] W. Buchmuller, V. Domcke, and K. Schmitz, *Phys. Lett. B* **811**, 135914 (2020), arXiv:2009.10649 [astro-ph.CO].
- [55] G. Lazarides, R. Maji, and Q. Shafi, *Phys. Rev. D* **108**, 095041 (2023), arXiv:2306.17788 [hep-ph].
- [56] Z. Wang, L. Lei, H. Jiao, L. Feng, and Y.-Z. Fan, *Sci. China Phys. Mech. Astron.* **66**, 120403 (2023), arXiv:2306.17150 [astro-ph.HE].
- [57] R. Samanta and S. Datta, *JHEP* **05**, 211 (2021), arXiv:2009.13452 [hep-ph].
- [58] L. Bian, J. Shu, B. Wang, Q. Yuan, and J. Zong, *Phys. Rev. D* **106**, L101301 (2022), arXiv:2205.07293 [hep-ph].
- [59] T. Hiramatsu, M. Kawasaki, and K. Saikawa, *JCAP* **02**, 031 (2014), arXiv:1309.5001 [astro-ph.CO].
- [60] L. Bian, R.-G. Cai, J. Liu, X.-Y. Yang, and R. Zhou, *Phys. Rev. D* **103**, L081301 (2021), arXiv:2009.13893 [astro-ph.CO].
- [61] R. Z. Ferreira, A. Notari, O. Pujolas, and F. Rompineve, *JCAP* **02**, 001 (2023), arXiv:2204.04228 [astro-ph.CO].
- [62] Y. Bai, T.-K. Chen, and M. Korwar, *JHEP* **12**, 194 (2023), arXiv:2306.17160 [hep-ph].
- [63] N. Kitajima, J. Lee, K. Murai, F. Takahashi, and W. Yin, *Phys. Lett. B* **851**, 138586 (2024), arXiv:2306.17146 [hep-ph].
- [64] S. Blasi, A. Mariotti, A. Rase, and A. Sevrin, *JHEP* **11**, 169 (2023), arXiv:2306.17830 [hep-ph].
- [65] Y. Li, L. Bian, and Y. Jia, (2023), arXiv:2304.05220 [hep-ph].
- [66] L. Bian, S. Ge, C. Li, J. Shu, and J. Zong, (2022), arXiv:2212.07871 [hep-ph].
- [67] E. Babichev, D. Gorbunov, S. Ramazanov, R. Samanta, and A. Vikman, *Phys. Rev. D* **108**, 123529 (2023), arXiv:2307.04582 [hep-ph].
- [68] A. S. Sakharov, Y. N. Eroshenko, and S. G. Rubin, *Phys. Rev. D* **104**, 043005 (2021), arXiv:2104.08750 [hep-ph].
- [69] Z. Zhang, C. Cai, Y.-H. Su, S. Wang, Z.-H. Yu, and H.-H. Zhang, *Phys. Rev. D* **108**, 095037 (2023), arXiv:2307.11495 [hep-ph].
- [70] A. Afzal et al. (NANOGrav), *Astrophys. J. Lett.* **951**, L11 (2023), arXiv:2306.16219 [astro-ph.HE].
- [71] L. Bian, S. Ge, J. Shu, B. Wang, X.-Y. Yang, and J. Zong, *Phys. Rev. D* **109**, L101301 (2024), arXiv:2307.02376 [astro-ph.HE].
- [72] Y. Bai and M. Korwar, *Phys. Rev. D* **105**, 095015 (2022), arXiv:2109.14765 [hep-ph].
- [73] F. Gao and I. M. Oldengott, *Phys. Rev. Lett.* **128**, 131301 (2022), arXiv:2106.11991 [hep-ph].
- [74] F. Gao, J. Harz, C. Hati, Y. Lu, I. M. Oldengott, and G. White, (2023), arXiv:2309.00672 [hep-ph].
- [75] Y. Lu, F. Gao, Y. X. Liu, and J. M. Pawlowski, (2023), to appear in *Phys. Rev. D*, arXiv:2310.18383 [hep-ph].
- [76] H. W. Zheng, Y. Lu, F. Gao, S. X. Qin, and Y. X. Liu, *Phys. Rev. D* **109**, 114013 (2024), arXiv:2312.00382 [hep-ph].
- [77] C. D. Roberts and A. G. Williams, *Prog. Part. Nucl. Phys.* **33**, 477 (1994), arXiv:hep-ph/9403224.
- [78] C. D. Roberts and S. M. Schmidt, *Prog. Part. Nucl. Phys.* **45**, S1 (2000), arXiv:nucl-th/0005064.
- [79] R. Alkofer and L. von Smekal, *Phys. Rept.* **353**, 281 (2001), arXiv:hep-ph/0007355.
- [80] C. S. Fischer, *J. Phys. G* **32**, R253 (2006), arXiv:hep-ph/0605173.
- [81] F. Gao, J. Papavassiliou, and J. M. Pawlowski, *Phys. Rev. D* **103**, 094013 (2021), arXiv:2102.13053 [hep-ph].
- [82] F. Gao and J. M. Pawlowski, *Phys. Rev. D* **102**, 034027 (2020), arXiv:2002.07500 [hep-ph].

- [83] P. J. Gunkel and C. S. Fischer, *Phys. Rev. D* **104**, 054022 (2021), [arXiv:2106.08356 \[hep-ph\]](#).
- [84] D. J. Schwarz and M. Stuke, *JCAP* **11**, 025 (2009), [Erratum: *JCAP* 10, E01 (2010)], [arXiv:0906.3434 \[hep-ph\]](#).
- [85] N. Aghanim et al. (Planck), *Astron. Astrophys.* **641**, A6 (2020), [Erratum: *Astron. Astrophys.* 652, C4 (2021)], [arXiv:1807.06209 \[astro-ph.CO\]](#).
- [86] C. Pitrou, A. Coc, J. P. Uzan, and E. Vangioni, *Phys. Rept.* **754**, 1 (2018), [arXiv:1801.08023 \[astro-ph.CO\]](#).
- [87] I. M. Oldengott and D. J. Schwarz, *EPL* **119**, 29001 (2017), [arXiv:1706.01705 \[astro-ph.CO\]](#).
- [88] L. A. Popa and A. Vasile, *JCAP* **06**, 028 (2008), [arXiv:0804.2971 \[astro-ph\]](#).
- [89] V. Simha and G. Steigman, *JCAP* **08**, 011 (2008), [arXiv:0806.0179 \[hep-ph\]](#).
- [90] P. D. Serpico and G. G. Raffelt, *Phys. Rev. D* **71**, 127301 (2005), [arXiv:astro-ph/0506162](#).
- [91] G. B. Gelmini, M. Kawasaki, A. Kusenko, K. Murai, and V. Takhistov, *JCAP* **09**, 051 (2020), [arXiv:2005.06721 \[hep-ph\]](#).
- [92] S. Pastor, T. Pinto, and G. G. Raffelt, *Phys. Rev. Lett.* **102**, 241302 (2009), [arXiv:0808.3137 \[astro-ph\]](#).
- [93] G. Mangano, G. Miele, S. Pastor, O. Pisanti, and S. Sarikas, *JCAP* **03**, 035 (2011), [arXiv:1011.0916 \[astro-ph.CO\]](#).
- [94] G. Mangano, G. Miele, S. Pastor, O. Pisanti, and S. Sarikas, *Phys. Lett. B* **708**, 1 (2012), [arXiv:1110.4335 \[hep-ph\]](#).
- [95] M. M. Middeldorf-Wygas, I. M. Oldengott, D. Bödeker, and D. J. Schwarz, *Phys. Rev. D* **105**, 123533 (2022), [arXiv:2009.00036 \[hep-ph\]](#).
- [96] R. Jinno and M. Takimoto, *Phys. Rev. D* **95**, 024009 (2017), [arXiv:1605.01403 \[astro-ph.CO\]](#).
- [97] M. Hindmarsh, S. J. Huber, K. Rummukainen, and D. J. Weir, *Phys. Rev. D* **92**, 123009 (2015), [arXiv:1504.03291 \[astro-ph.CO\]](#).
- [98] J. R. Espinosa, T. Konstandin, J. M. No, and G. Servant, *JCAP* **06**, 028 (2010), [arXiv:1004.4187 \[hep-ph\]](#).
- [99] J. Ellis, M. Lewicki, and J. M. No, *JCAP* **07**, 050 (2020), [arXiv:2003.07360 \[hep-ph\]](#).
- [100] J. Ellis, M. Lewicki, J. M. No, and V. Vaskonen, *JCAP* **06**, 024 (2019), [arXiv:1903.09642 \[hep-ph\]](#).
- [101] H. K. Guo, K. Sinha, D. Vagie, and G. White, *JCAP* **01**, 001 (2021), [arXiv:2007.08537 \[hep-ph\]](#).
- [102] D. J. Weir, *Phil. Trans. Roy. Soc. Lond. A* **376**, 20170126 (2018), [Erratum: *Phil. Trans. Roy. Soc. Lond. A* 381, 20230212 (2023)], [arXiv:1705.01783 \[hep-ph\]](#).
- [103] R. W. Haymaker, T. Matsuki, and F. Cooper, *Phys. Rev. D* **35**, 2567 (1987).
- [104] S. R. Coleman, *Phys. Rev. D* **15**, 2929 (1977), [Erratum: *Phys. Rev. D* 16, 1248 (1977)].
- [105] A. D. Linde, *Phys. Lett. B* **100**, 37 (1981).
- [106] A. D. Linde, *Nucl. Phys. B* **216**, 421 (1983), [Erratum: *Nucl. Phys. B* 223, 544 (1983)].
- [107] J. Ellis, M. Lewicki, and J. M. No, *JCAP* **04**, 003 (2019), [arXiv:1809.08242 \[hep-ph\]](#).
- [108] D. Bödeker and G. D. Moore, *JCAP* **05**, 009 (2009), [arXiv:0903.4099 \[hep-ph\]](#).
- [109] C. Caprini et al., *JCAP* **04**, 001 (2016), [arXiv:1512.06239 \[astro-ph.CO\]](#).
- [110] D. J. Reardon et al., *Astrophys. J. Lett.* **951**, L7 (2023), [arXiv:2306.16229 \[astro-ph.HE\]](#).
- [111] A. Zic et al., *Publ. Astron. Soc. Austral.* **40**, e049 (2023), [arXiv:2306.16230 \[astro-ph.HE\]](#).
- [112] G. Agazie et al. (NANOGrav), *Astrophys. J. Lett.* **951**, L9 (2023), [arXiv:2306.16217 \[astro-ph.HE\]](#).
- [113] F. Gao, J. Chen, Y. X. Liu, S. X. Qin, C. D. Roberts, and S. M. Schmidt, *Phys. Rev. D* **93**, 094019 (2016), [arXiv:1507.00875 \[nucl-th\]](#).
- [114] P. Isserstedt, M. Buballa, C. S. Fischer, and P. J. Gunkel, *Phys. Rev. D* **100**, 074011 (2019), [arXiv:1906.11644 \[hep-ph\]](#).
- [115] W. J. Fu and J. M. Pawłowski, *Phys. Rev. D* **92**, 116006 (2015), [arXiv:1508.06504 \[hep-ph\]](#).
- [116] Y. Lu, F. Gao, B. C. Fu, H. C. Song, and Y. X. Liu, (2023), [arXiv:2310.16345 \[hep-ph\]](#).
- [117] C. S. Fischer, J. Luecker, and C. A. Welzbacher, *Phys. Rev. D* **90**, 034022 (2014), [arXiv:1405.4762 \[hep-ph\]](#).
- [118] O. Philipsen, *Prog. Part. Nucl. Phys.* **70**, 55 (2013), [arXiv:1207.5999 \[hep-lat\]](#).
- [119] J. N. Guenther, R. Bellwied, S. Borsanyi, Z. Fodor, S. D. Katz, A. Pasztor, C. Ratti, and K. K. Szabó, *Nucl. Phys. A* **967**, 720 (2017), [arXiv:1607.02493 \[hep-lat\]](#).
- [120] A. Eichhorn, J. Lumma, J. M. Pawłowski, M. Reichert, and M. Yamada, *JCAP* **05**, 006 (2021), [arXiv:2010.00017 \[hep-ph\]](#).

Supplemental Material

I. THERMAL QUANTITIES AND COSMIC TRAJECTORY DURING THE QCD TRANSITION

At finite temperature and chemical potential, the general form of the solution of the quark DSE can be expressed as:

$$S^{-1}(\tilde{\omega}_n, \vec{p}) = i\vec{\gamma} \cdot \vec{p}A(\tilde{\omega}_n, \vec{p}) + i\gamma_4\tilde{\omega}_nC(\tilde{\omega}_n, \vec{p}) + B(\tilde{\omega}_n, \vec{p}). \quad (13)$$

with \vec{p} the momentum, $\tilde{\omega}_n = \omega_n + i\mu_q$, $\omega_n = (2n+1)\pi T$ the Matsubara frequency and μ_q the quark chemical potential. Then, the dynamic quark mass is defined as:

$$M_q = \text{Re} \left[\frac{B(\tilde{\omega}_0, \vec{p}=0)}{C(\tilde{\omega}_0, \vec{p}=0)} \right]. \quad (14)$$

The thermal quantities of QCD, including the number density and the entropy density, can be obtained by solving DSE [75, 113, 114]. The quark number density n_q and the entropy s can be written as:

$$n_q = \frac{\partial P}{\partial \mu_q}, \quad (15)$$

$$s = \frac{\partial P}{\partial T}, \quad (16)$$

with P the pressure and μ_q the quark chemical potential. The number density of u/d and s quark can be expressed in terms of the dynamical quark mass M_q and the traced Polyakov loop Φ in phase diagram (T, μ_q) plane [115, 116]:

$$n_q(T, \mu_q) = 2N_c \int \frac{d^3k}{(2\pi)^3} [f_q^+(k; T, \mu_q) - f_q^-(k; T, \mu_q)], \quad (17a)$$

$$f_q^\pm(k; T, \mu_q) = \frac{\Phi(T, \mu_q)x_\pm^2 + 2\Phi(T, \mu_q)x_\pm + 1}{x_\pm^3 + 3\Phi(T, \mu_q)x_\pm^2 + 3\Phi(T, \mu_q)x_\pm + 1}, \quad (17b)$$

$$x_\pm(k; T, \mu_q) = \exp[(E_q(k; T, \mu_q) \mp \mu_q)/T], \quad (17c)$$

$$E_q(k; T, \mu_q) = \sqrt{k^2 + M_q^2}, \quad (17d)$$

with N_c the color number. The traced Polyakov loop Φ at vanishing quark chemical potential is parameterized as [116, 117]:

$$\Phi(T, \mu_q) = L(t_{\mu_q}), \quad (18a)$$

$$t_{\mu_q} = \frac{T}{T_c(0)} + \kappa \left(\frac{3\mu_q}{T_c(0)} \right)^2, \quad (18b)$$

$$L(t) = \frac{2}{1 + \exp\left(\frac{a_1 + b_1 t^3}{t + c_1 t^3 + d_1 t^6}\right)}, \quad (18c)$$

where $T_c(0) = 155.2 \text{ MeV}$ the PT temperature at vanishing chemical potential and $\kappa = 0.0184$ the curvature of the transition line. The fit parameters are $[a_1, b_1, c_1, d_1] = [2.5996, -0.2046, -1.2346, 2.2308]$. From the definition of the Eq. (15) and the Eq. (16), the chemical potential dependence of the entropy density can be expressed as the integral along μ_q [75]:

$$\delta s(T, \mu) = s(T, \mu) - s(T, 0) = \int_0^{\mu_q} d\mu_q' \frac{\partial n_q(T, \mu')}{\partial T}. \quad (19)$$

To include the gluon pressure, we use the lattice QCD results to obtain the entropy density at vanishing chemical potential as parametrized in the lattice QCD [118]. The full entropy density can then be expressed as:

$$s_{QCD}(T, \mu) = s_{latt}(T, \mu=0) + \delta s(T, \mu). \quad (20)$$

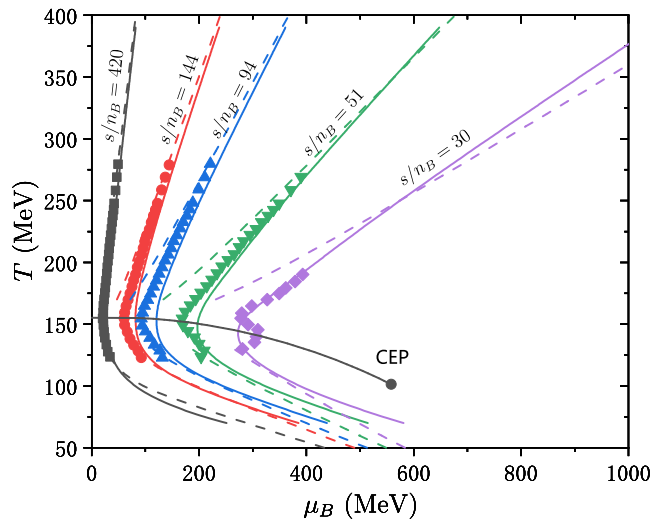


FIG. 5. Isentropic trajectories at $s/n_B = 420, 144, 94, 51$ and 30 . Solid line: DSE from this work; scatter points: the lattice [119]; dashed line (above): the improved ideal quark gas; dashed line (below): HRG. The solid line with a point represents the crossover of QCD phase transition, with the point corresponding to the critical end point (CEP).

We compare the isentropic trajectories $s/n_B = \text{const}$ from DSE with the result of the improved ideal quark gas, HRG and the lattice in Fig. (5), showing an well consistency. The improved ideal quark gas includes the lattice QCD entropy $s_{latt}(T, \mu = 0)$ in Eq. (20), and apply the Fermi-Dirac distribution for the quark number densities. The application of $s_{latt}(T, \mu = 0)$ is due to the gluons do not behave like the idea gas in the QCD phase transition region. The consistency shown in Fig. (5) makes the calculation of the five conserve equations in Eq. (1) of the cosmic trajectories more reliable, because these equations also satisfies a form similar to $s/n_B = \text{const}$.

During the cosmic QCD transition, the kinetic and the chemical equilibrium are excellent approximation [120]. The $2 \leftrightarrow 2$ process is the primary mechanism, responsible for establishing both kinetic and chemical equilibrium among all particles, which constrains the chemical potentials of leptons as $\mu_\mu = \mu_e - \mu_{\nu_e} + \mu_{\nu_\mu}$, and the leptons and quarks as $\mu_d = \mu_e - \mu_{\nu_e} + \mu_u$. Chemical equilibrium constrains the chemical potentials of different particle species to only five independent chemical potentials for the universe. The chemical potentials of photons and gluons are zero because the numbers of photons and gluons are not conserved. The chemical potentials of particles and antiparticles are equal in magnitude, but opposite in sign. For instance, if a particle has a chemical potential of μ_i , its antiparticle has a chemical potential of $-\mu_i$. Due to flavor mixing, we only need to distinguish the chemical potentials of up and down quarks: $\mu_u = \mu_c = \mu_t$, and $\mu_d = \mu_s = \mu_b$ [84]. Therefore we are left with $\mu_u, \mu_e, \mu_{\nu_e}, \mu_{\nu_\mu}, \mu_{\nu_\tau}$ as the independent variables for the cosmic trajectory. Then the chemical potentials of conserved charges (Y_{L_f}, Y_B, Q) can be expressed in terms of particle chemical potential as:

$$\mu_{L_f} = \mu_{\nu_f}, \quad (21a)$$

$$\mu_Q = \mu_u - \mu_d, \quad (21b)$$

$$\mu_B = \mu_u + 2\mu_d. \quad (21c)$$

Then the temperature dependence of the five chemical potentials (μ_{L_f}, μ_Q, μ_B) are the cosmic trajectory. We will focus on the (T, μ_q) plane in QCD phase diagram, especially in the first-order phase transition region, where the CEP locates at $(T^E, \mu_q^E) = (101.3, 186.0)$ MeV.

In the scenario ($Y_{L_e} = 0, Y_{L_\mu} = -Y_{L_\tau}$), for a specific value, such as $Y_{L_\mu} = -0.45$, the cosmic trajectory follows a path from a to d , crossing the QCD FOPT region illustrated in Fig. 6. During the a - b period, the false vacuum energy of the universe is lower, rendering the false vacuum more stable. At this stage, the universe is filled with the false vacuum, which is also referred to as the Wigner vacuum in QCD. In the subsequent b - c period, the energy of the false vacuum exceeds that of the true vacuum, yet both are in local minima. During this period, the false vacuum is a supercooled phase, meaning the universe remaining filled with the false vacuum. At the point c , the false vacuum initiates the decay into the true vacuum, leading to the nucleation and the percolation of bubbles. The c - d process remains unclear, since the non-equilibrium processes are not calculated currently, while the cosmic trajectories involving the non-equilibrium processes can be constrained within the shadow area. This shadowed area is bounded

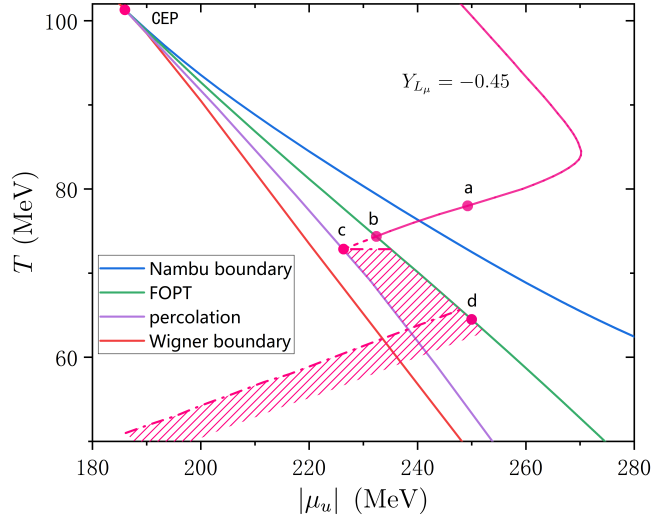


FIG. 6. The cosmic trajectory across the first-order phase transition region in the scenario $Y_{L_e} = 0, Y_{L_\mu} = -Y_{L_\tau}$, where $Y_{L_\mu} = -0.45$. Solid line: the specific cosmic trajectory, such as a - b ; dashed line: the supercooling stage for a cosmic trajectory before the percolation and after the FOPT, such as b - c ; dot-dashed line: the upper bound for the possible cosmic trajectory; shadow region: an area through which a cosmic trajectory may pass.

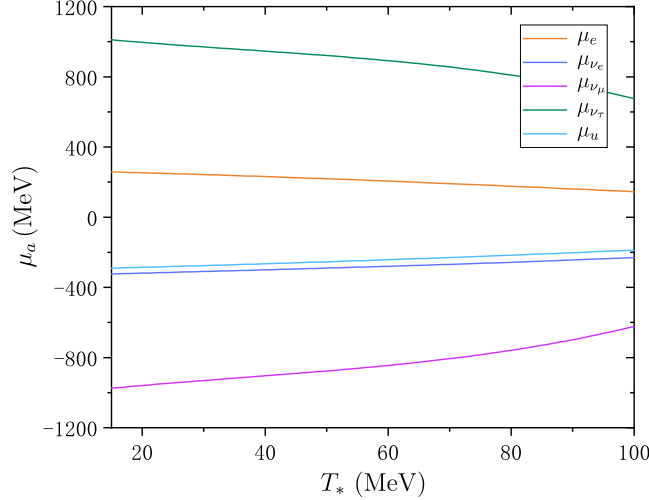


FIG. 7. The lepton and quark chemical potentials on the percolation line.

by an upper limit but remains unconstrained by a lower limit. The dot-dashed line above the point d represents the upper bound of the cosmic trajectory. This upper bound is calculated under the conservation of s/n before and after the phase transition, while s/n could increase in general through the non-equilibrium processes. This upper bound is determined by the thermal quantities of the true vacuum. As one approaches the point d , the Gibbs phase equilibrium condition requires the cosmic trajectory aligns with the FOPT line. At the point d , the universe is filled with the true vacuum just at this moment. During the process from the point c to d , quarks gain a large mass due to the dynamic chiral symmetry breaking, which then suppresses the quark number density of the true vacuum, rendering the cosmic trajectory to be shifted below that of the false vacuum.

Fig. 7 shows the lepton and quark chemical potentials on the percolation line. The lepton chemical potentials are large because of the conservation conditions in Eq. (1). This, in turn, causes α_* to be small due to the large energy density of the background radiation.

II. PT PARAMETERS OF GRAVITATIONAL WAVES AT FINITE TEMPERATURE AND CHEMICAL POTENTIAL

A critical value of α , which can determine whether the bubble walls can runaway, is defined as [100]:

$$\alpha_\infty = \frac{\Delta P_{LO}}{\rho_r}, \quad (22)$$

where [108]

$$\Delta P_{LO} = \sum_{a'} \int_{m_f}^{m_t} dm^2 \int \frac{d^3p}{(2\pi)^3} \frac{f_{F/B}(E, T, \mu_{a'})}{2E}, \quad (23)$$

with $\sum_{a'}$ summing over all particles taking part in the phase transition, m_f (m_t) the particle mass in false (true) vacuum and $f_{F/B}$ the Fermi–Dirac (Bose–Einstein) distribution function.

To obtain the PT parameters that take the derivative along the cosmic trajectory at finite temperature and chemical potential, we start with the fluid equation:

$$\dot{\rho}_r + 3\frac{\dot{a}}{a}(\rho_r + p) = 0, \quad (24)$$

with

$$p = \frac{1}{3}\rho_r, \quad (25)$$

with a the scale factor, ρ_r the energy density of radiation and p the pressure. Eq. (25) is valid even for radiation in finite chemical potential. The term ρ_r considers only the radiation (except for muon due to its mass is close to the PT temperature), because the matter energy density is much smaller than that of the radiation. The u/d quarks in the false vacuum, instead of the true vacuum, are considered in ρ_r because the decay rate $\Gamma(T, \mu)$ is that of the false vacuum. Combining Eq. (24) and Eq. (25), we obtain:

$$dt = -\frac{d\rho_r}{4H\rho_r}, \quad (26)$$

$$\rho_r = \rho_{r0}a^{-4}, \quad (27)$$

with t the time along the cosmic trajectory, $H = \frac{\dot{a}}{a}$ the Hubble parameter and ρ_{r0} the energy density at a given time.

The probability that a point still remains in the false vacuum is written as [107]:

$$P(t) = e^{-I(t)}, \quad (28)$$

$$I(t) = \frac{4\pi}{3} \int_{t_c}^t dt' \Gamma(t') a(t')^3 \left(\int_{t'}^t \frac{v_w dt''}{a(t'')} \right)^3. \quad (29)$$

After that, the formula to determine the percolation temperature and chemical potential (T_* , μ_*) can be derived by applying Eq. (26) and Eq. (27) to Eq. (29):

$$I(T, \mu) = \frac{4\pi}{3} \int_{\rho_r}^{\rho_r^c} d\rho_r' \frac{1}{4\rho_r'^{7/4}} \frac{\Gamma(T', \mu')}{H(T', \mu')} \times \left(\int_{\rho_r}^{\rho_r'} d\rho_r'' \frac{v_w}{4H(T'', \mu'') \rho_r''^{3/4}} \right)^3. \quad (30)$$

Similarly, the inverse PT duration β/H_* can be derived with Eq. (26):

$$\beta = -\frac{d}{dt} \left(\frac{S_3}{T} \right) \Big|_{t_*} = 4H_* \rho_r \frac{d}{d\rho_r} \left(\frac{S_3}{T} \right) \Big|_{(T_*, \mu_*)}, \quad (31)$$

where the derivative lies along the cosmic trajectory.